Rapid Communications | Editors' Suggestion

Observation of strong higher-order lattice anharmonicity in Raman and infrared spectra

Xiaolong Yang,[1,2,3,*] Tianli Feng,[1,*] Joon Sang Kang,[4] Yongjie Hu,[4] Ju Li,[5] and Xiulin Ruan[1,†]

[1]*School of Mechanical Engineering and the Birck Nanotechnology Center, Purdue University, West Lafayette, Indiana 47907-2088, USA*

[2]*Institute for Advanced Study, Shenzhen University, Shenzhen 518060, China*

[3]*Frontier Institute of Science and Technology, and State Key Laboratory for Mechanical Behavior of Materials, Xi'an Jiaotong University, Xi'an 710049, China*

[4]*School of Engineering and Applied Science, University of California, Los Angeles (UCLA), Los Angeles, California 90095, USA*

[5]*Department of Nuclear Science and Engineering and Department of Materials Science and Engineering, Massachusetts Institute of Technology, Cambridge, Massachusetts 02139, USA*

(Received 6 December 2018; revised manuscript received 13 September 2019; accepted 10 March 2020; published 6 April 2020)

The fundamental theory of Raman and infrared (IR) linewidth has been well established as the third-order lattice anharmonicity (three-phonon scattering). In this work, we use both rigorous density functional calculations and Raman experiments to find, surprisingly, that the fourth-order anharmonicity universally plays a significant or even dominant role over the third-order anharmonicity at room temperature, and more so at elevated temperatures, for a wide range of materials including diamond, Si, Ge, GaAs, boron arsenide (BAs), cubic silicon carbide (3*C*-SiC), and α-quartz. This is enabled by the large four-phonon scattering phase space of zone-center optical phonons. Raman measurements on BAs were conducted, and their linewidth verifies our predictions. The predicted infrared optical properties through the Lorentz oscillator model, after including four-phonon scattering, show much better agreement with experimental measurements than those three-phonon-based predictions. Our work advances the fundamental understanding of Raman and IR response and will broadly impact spectroscopy techniques and radiative transport.

DOI: 10.1103/PhysRevB.101.161202

Phonon anharmonicity plays a key role in the linewidth of infrared and Raman spectra, which are basic material properties important for sensing, materials characterizations, radiative heat transfer including near-field radiation and radiative cooling, energy harvesting, and metamaterials [1,2]. It is also key to the dielectric function of polar dielectrics in the IR range, which can be effectively described by the Lorentz oscillator model [2]:

$$\epsilon(\omega) = \epsilon_\infty \left(1 + \sum_m \frac{\omega_{\mathrm{LO},m}^2 - \omega_{\mathrm{TO},m}^2}{\omega_{\mathrm{TO},m}^2 - \omega^2 - i\gamma_m\omega}\right), \qquad (1)$$

where ϵ_∞ is the dielectric constant at the high-frequency limit, ω is the photon frequency, ω_{TO} and ω_{LO} are frequencies of the zone-center TO (transverse optical) and LO (longitudinal optical) phonon modes, respectively, γ is the damping factor manifesting phonon anharmonicity and is equal to the zone-center optical phonon linewidth 2Γ, and m is the index of all the IR-active zone-center phonon modes. Phonon linewidth is generally difficult to measure at high temperatures due to thermal oxidation and self-radiation [3]. The available measured zone-center optical phonon linewidths have been explained in the framework of third-order phonon anharmonicity (three-phonon scattering) [4–9]. However, the predicted linewidths are considerably smaller than the experimental data, e.g., silicon at high temperature [4] and zinc-blende GaAs at room temperature [6], and the discrepancy was attributed to defect or impurity scattering. An attempt to include higher-order scattering through *ab initio* molecular dynamics [10] did not improve over the density-functional perturbation theory (DFPT) based on three-phonon scattering. A recent DFPT incorporating four-phonon scattering [11] considerably overestimated the zone-center phonon linewidth, which is difficult to interpret since the predicted intrinsic linewidth corresponds to a pristine crystal and should serve as a lower limit for experiments. Hence, the role of higher-order anharmonicity is still unclear.

In this work, we perform density functional theory calculations and Raman experiments to directly show that strong or even dominant higher-order phonon anharmonicity, not defects or impurities, is responsible for the larger-than-expected Raman and IR linewidth for a *wide* range of materials including diamond, Si, Ge, GaAs, BAs, 3*C*-SiC, and α-quartz at various temperatures. In many of the situations higher-order anharmonicity is negligible for acoustic phonons and thermal conductivity, but important for zone-center optical phonons and hence Raman and IR response. The phonon properties are predicted from the vibrational Hamiltonian, which can be Taylor expanded as $\hat{H} = \hat{H}_0 + \hat{H}_3 + \hat{H}_4 + \cdots$, where $\hat{H}_0$, $\hat{H}_3$, and $\hat{H}_4$ are the harmonic, cubic, and quartic terms, respectively. $\hat{H}_3$ induces the phonon linewidth by three-phonon scattering rates $\tau_{3,\lambda}^{-1}$ [12–14]. $\hat{H}_4$ induces four-phonon scattering rates $\tau_{4,\lambda}^{-1}$ [15–17]. We also include the effect of phonon-isotope scattering τ_{iso}^{-1} on the phonon linewidth [18].

*These authors contributed equally to this work.
†Corresponding author: ruan@purdue.edu.

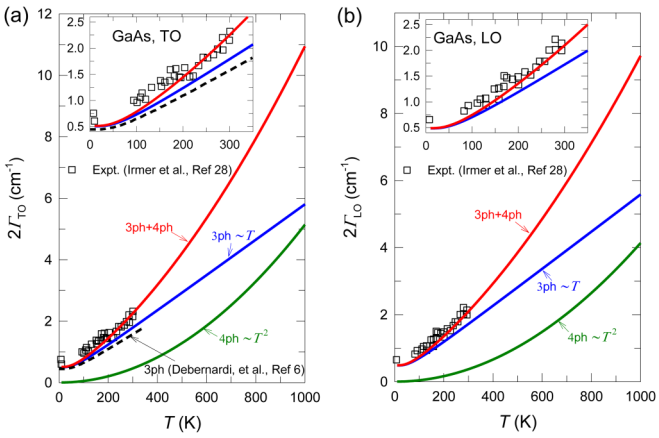

FIG. 1. T dependence of the phonon linewidth, 2Γ, of the TO (a) and LO (b) modes in GaAs, with the insets for a better view below 300 K. The solid lines represent the results of the present calculation; the dashed lines denote the calculated result from Ref. [6]; the squares denote experimental data from Ref. [28].

Here the phonon linewidth is calculated under the single mode relaxation time approximation (SMRTA) by directly summing the normal and umklapp scattering rates. The phonon linewidth is associated with the decay rate of a phonon after its single mode excitation, where normal scattering contributes in a similar manner with the umklapp scattering. Therefore, SMRTA has been shown to generally work well for the prediction of phonon linewidth [4,19]. It can be noted that for thermal conductivity, on the other hand, umklapp scattering directly contributes to thermal resistance while normal scattering only indirectly contributes. Hence for predicting thermal conductivity, the SMRTA works for materials where umklapp scattering dominates, while the iterative approach should be used for materials with large normal scattering rates (such as diamond) [20]. Here the full width at half maximum 2Γ of a phonon mode is calculated as a Matthiessen sum of contributions from isotope scattering, three-phonon scattering, and four-phonon scattering rates:

$$2\Gamma = \gamma = \tau_{\text{iso}}^{-1} + \tau_{3,\lambda}^{-1} + \tau_{4,\lambda}^{-1}. \tag{2}$$

The formalism described above requires the second-, third-, and fourth-order interatomic force constants for calculating phonon frequencies and scattering rates, which were obtained from the Vienna *Ab initio* Simulation Package (VASP) [21] within the local density approximation, with the details given in Sec. A of the Supplemental Material [22]. Specifically, we use the four-phonon scattering formalism in Refs. [15–17], which has been validated by recent experiments on the high thermal conductivity of BAs [23–25] and extended to strongly anharmonic materials [26,27]. Our predicted phonon dispersions of all materials studied agree well with those measured in the literature as shown in Sec. B of the Supplemental Material [22] (see, also, Refs. [7–12] therein).

Taking GaAs as an example, we show the calculated T-dependent TO phonon linewidth in Fig. 1(a) with the inset for a better view below $T_{\text{room}} = 300$ K. Isotope scattering is included in all curves in this Rapid Communication unless noted otherwise. We find that the three-phonon scattering prediction is considerably lower than the experimental data [28] even at T_{room}. With $\tau_{4,\lambda}^{-1}$ included, the prediction matches with experiment surprisingly well. Note that four-phonon scattering is negligible for thermal conductivity of GaAs at T_{room} [29,30]. Also, as T increases, our prediction of 2Γ including $\tau_{4,\lambda}^{-1}$ deviates significantly from that only involving $\tau_{3,\lambda}^{-1}$, as shown in Fig. 1(a). This indicates that four-phonon processes, which were neglected in the past, can actually remedy the discrepancies between previous calculations [6] and experiments. We also note that $\tau_{3,\lambda}^{-1}$ increases approximately linearly, whereas $\tau_{4,\lambda}^{-1}$ increases approximately quadratically with increasing T, consistent with Refs. [15,31]. Thus, $\tau_{4,\lambda}^{-1}$ becomes comparable to $\tau_{3,\lambda}^{-1}$ at mid to high temperatures. Similar significance of four-phonon scattering is also found for the LO branch as shown in Fig. 1(b).

Figure 2 shows the T-dependent optical phonon linewidths for diamond, Si, Ge, BAs, 3C-SiC, and α- quartz, respectively. Similarly, only after including four-phonon scattering can we see good agreements with available experimental data from Refs. [32–38] and our own Raman spectra of BAs (see Sec. C of the Supplemental Material [22] for details). The difference between our three-phonon prediction and the previous calculation [4] in diamond is attributed to the isotope effect, which was not included in Ref. [4]. It should be noted that, unlike other materials, the experimental Raman spectra of BAs contain strong influence from isotope scattering [39]. We have subtracted such background contribution from both the experimental and the theoretical data, to leave only the T-dependent anharmonic linewidth for comparison. The agreement between prediction and experiment is excellent. It can be seen that in BAs the three-phonon processes have little contribution to the zone-center TO phonon linewidth due to lack of allowed scattering, and the four-phonon scattering totally dominates over three-phonon scattering in the entire T range. It should be noted that the T-induced phonon renormalization [40] may also affect phonon linewidths, which is not dealt with in the present work, but is non-negligible above the Debye temperature.

To gain a deeper insight into the microscopic mechanisms, we further analyze the contribution to $\tau_{4,\lambda}^{-1}$ from different scattering channels using BAs as an example. In Fig. 3(a), it can be seen that the dominant decay channels for zone-center optical phonons are the recombination process $\lambda_1 + \lambda_2 \rightarrow \lambda_3 + \lambda_4 + \mathbf{K}$, where $\mathbf{K}$ is a reciprocal lattice vector, which is zero for normal processes and nonzero for umklapp processes. These processes contribute more than 90% to $\tau_{4,\lambda}^{-1}$ of the zone-center optical phonon of BAs at 1000 K. Similar cases are also found in the other materials studied. The origin of such high $\tau_{4,\lambda}^{-1}$ of optical branches is illustrated in Fig. 3(b). The optical branches bunch together and allow the four modes λ_1, λ_2, λ_3, and λ_4 to have similar energies. Alternatively, the summation of the energies of an optical phonon λ_1 and an acoustic phonon λ_2 can easily reach that of another optical phonon λ_3 and another acoustic phonon λ_4. Therefore, the energy conservation rule for the recombination process $\lambda_1 + \lambda_2 \rightarrow \lambda_3 + \lambda_4 + \mathbf{K}$ is easily satisfied. As a result, the optical branches often have large four-phonon scattering phase space. This is a key difference for phonon linewidth as compared to thermal transport, which is dominated by acoustic phonons

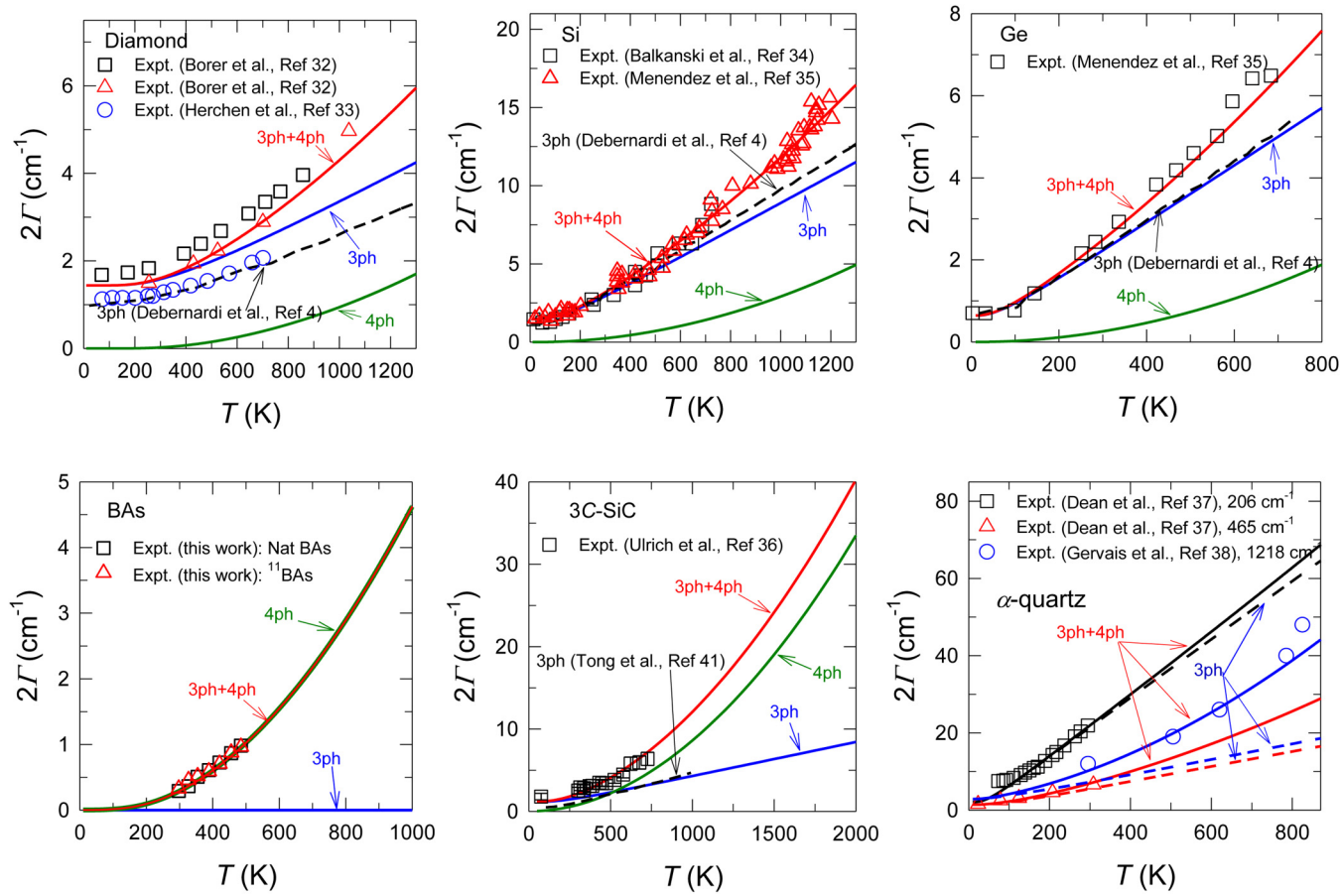

FIG. 2. Zone-center optical phonon linewidth in diamond, Si, Ge, BAs, 3C-SiC, and α-quartz as a function of T. For diamond, Si, and Ge, the solid curves represent the results of the present calculation, and the dashed curves denote the calculated results from Ref. [4]; all symbols denote experimental data from Refs. [32–35]. For BAs, the solid curves represent the results of our present calculations of the TO phonon linewidth; the black squares and red up triangles denote our Raman measurement for natural abundance and isotope pure BAs, respectively. For 3C-SiC, the solid curves represent our present prediction of the TO phonon linewidth; the black squares denote experimental data from Ref. [36]; the dashed curve represents the calculated result from Ref. [41]. For α-quartz, all curves represent our predicted phonon linewidth with (solid lines) and without (dashed lines) $\tau_{4,\lambda}^{-1}$ for phonon modes with frequencies of 206, 465, and 1218 cm^{-1}, and all symbols denote the experimental data from Refs. [37,38].

and strongly depends on the temperature, acoustic-optical gap, and anharmonicity of the materials. In other words, the significance of four-phonon scattering will be more broadly seen in zone-center optical phonon linewidth than in thermal conductivity.

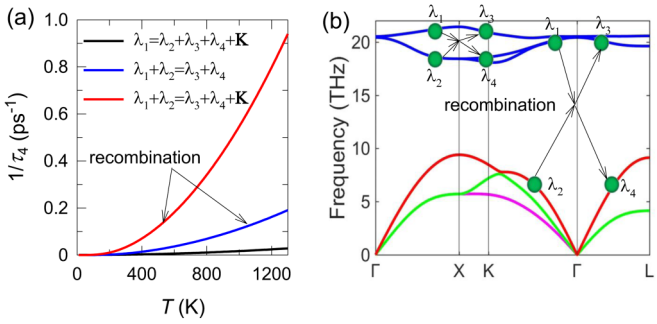

FIG. 3. (a) The contribution to $\tau_{4,\lambda}^{-1}$ of BAs from different scattering channels. (b) Phonon dispersion of BAs with schematic diagrams of four-phonon scattering processes dominated by recombination channels.

With the predicted 2Γ combined with frequency values ω_{TO} and ω_{LO} listed in Supplemental Material Table S1 [22] (see, also, Refs. [12–16] therein), we address the importance of four-phonon scattering in dielectric function ϵ. The calculated ϵ with $\tau_{4,\lambda}^{-1}$ (red lines) for BAs, and the calculated ϵ with (red lines) and without (blue lines) $\tau_{4,\lambda}^{-1}$ for 3C-SiC and α-quartz at various T, are presented in Fig. 4(a). Here isotope scattering is excluded in BAs to make the anharmonic effects stand out. Remarkably, for isotopically pure BAs, the three-phonon scattering has almost no contribution and four-phonon scattering completely dominates the imaginary part of the dielectric function, ϵ_i. For 3C-SiC, with $\tau_{4,\lambda}^{-1}$ included the ϵ_i has a much broader peak, corresponding to a larger linewidth as highlighted by the solid arrow. We also find that when four-phonon scattering is added the peak value of ϵ_i decreases by 70% for 3C-SiC at 1000 K. For α-quartz, after introducing $\tau_{4,\lambda}^{-1}$, the peak values of the dielectric function at 785 K also have a significant reduction ranging from 20% to 50%

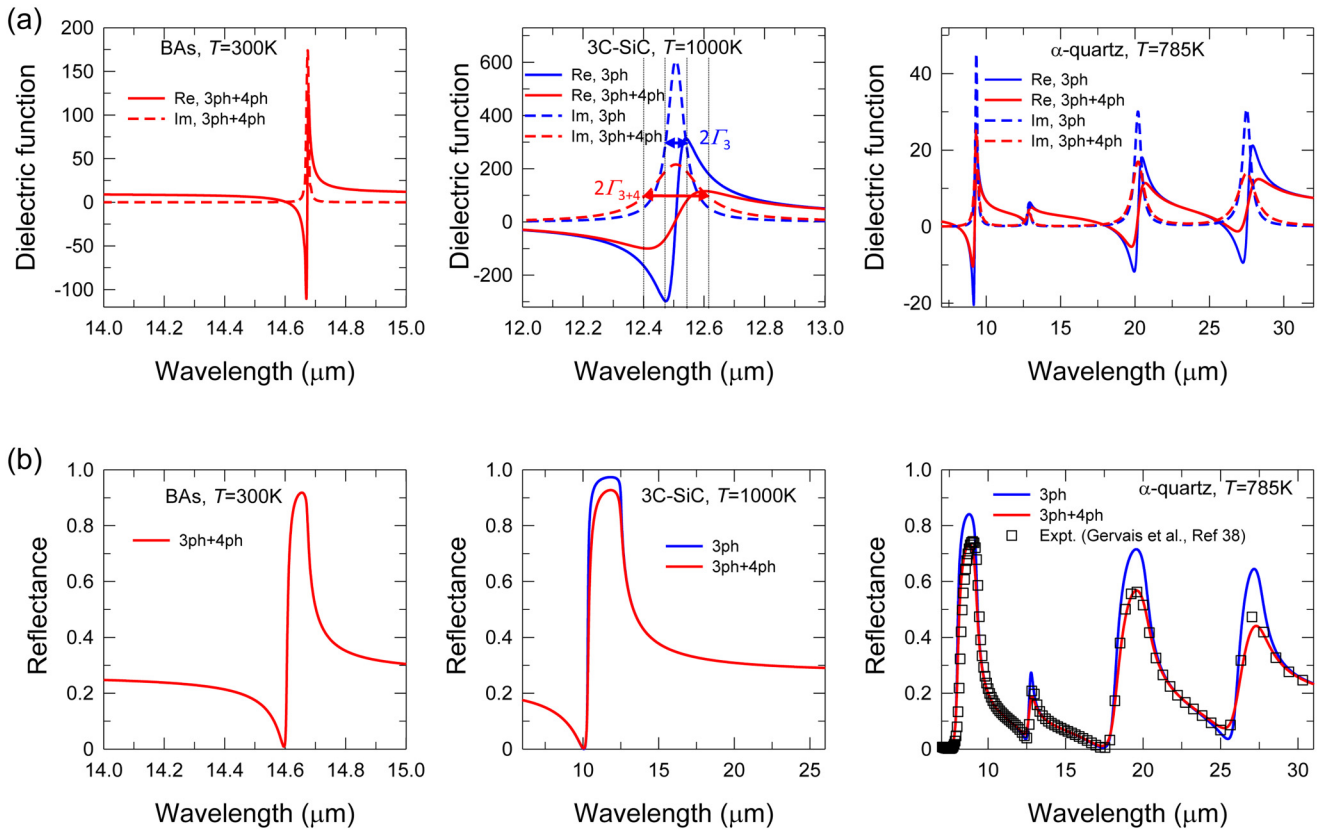

FIG. 4. (a) The calculated dielectric function of BAs, 3*C*-SiC, and α-quartz with (red lines) and without (blue lines) $\tau_{4,\lambda}^{-1}$ included. Solid lines represent the real part (Re) of dielectric function and dashed lines denote the imaginary part (Im) of dielectric function. (b) The calculated semi-infinite normal reflectance R for BAs at 300 K, 3*C*-SiC at 1000 K, and α-quartz at 785 K along with available experimental data [38] for comparison.

for different vibrational modes. These results suggest that previous works that considered three-phonon anharmonicity alone led to significant errors, and four-phonon scattering plays a decisive role in predicting high-temperature dielectric functions of IR-active materials.

With the complex dielectric function ϵ, the normal reflectance from a semi-infinite block R can be calculated as $R(\omega) = |(\sqrt{\epsilon(\omega)} - 1)/(\sqrt{\epsilon(\omega)} + 1)|^2$. In Fig. 4(b), we show our predicted reflectance R of BAs, 3*C*-SiC, and α-quartz at various T, and the latter is compared to the available experimental measurement in Ref. [38]. It is found that at T_{room} our four-phonon theory predicts the peak value of pure BAs reflectivity as much as $\sim$0.9, which offers an important theoretical basis for experimental measurements. For 3*C*-SiC, with four-phonon scattering included, the peak of reflectivity in the range of 10–13 μm will reduce by 10%. For α-quartz, it can be observed that the predicted reflectance peak with $\tau_{4,\lambda}^{-1}$ decreases by 10%–30% as compared to that with only $\tau_{3,\lambda}^{-1}$, and matches exceptionally well with the existing IR data [38].

In conclusion, we have observed strong or even dominating fourth-order phonon anharmonicity in Raman and IR response by first-principles calculations and Raman measurements. Our results on a series of technically important semiconductors demonstrate that the previously neglected four-phonon scattering generally dominates optical phonon linewidth at elevated and high temperatures, owing to the relatively large density of states and four-phonon scattering phase space of the zone-center optical phonons. With four-phonon scattering included, the infrared optical properties of α-quartz agree well with previous measurements. Our work thus reveals a crucial role of four-phonon scattering for zone-center optical phonons as in Raman and IR response.

T.F. and X.R. acknowledge the partial support from the Defense Advanced Research Projects Agency (Award No. HR0011-15-2-0037) and the School of Mechanical Engineering, Purdue University. X.Y. acknowledges the support from the China Scholarship Council under Grant No. 201706280325 and the China Postdoctoral Science Foundation under Grant No. 2019M663028. J.L. acknowledges support by an Office of Naval Research MURI grant N00014-17-1-2661. Y.H. acknowledges support from a CAREER Award from the National Science Foundation under Grant No. 1753393. Simulations have been performed at the Rosen Center of Advanced Computing at Purdue University.

[1] M. Born and K. Huang, *Dynamical Theory of Crystal Lattices*, International Series of Monographs on Physics (Clarendon, Oxford, 1988).

[2] Z. Zhang, *Nano/Microscale Heat Transfer* (McGraw-Hill, New York, 2007).

[3] H. Fujiwara, *Ellipsometry of Anisotropic Materials* (John Wiley & Sons, Ltd., New York, 2007).

[4] A. Debernardi, S. Baroni, and E. Molinari, Phys. Rev. Lett. **75**, 1819 (1995).

[5] G. Lang, K. Karch, M. Schmitt, P. Pavone, A. P. Mayer, R. K. Wehner, and D. Strauch, Phys. Rev. B **59**, 6182 (1999).

[6] A. Debernardi, Phys. Rev. B **57**, 12847 (1998).

[7] A. Debernardi, C. Ulrich, K. Syassen, and M. Cardona, Phys. Rev. B **59**, 6774 (1999).

[8] F. Bechstedt, P. Käckell, A. Zywietz, K. Karch, B. Adolph, K. Tenelsen, and J. Furthmüller, Phys. Status Solidi B **202**, 35 (1997).

[9] X. Tang and B. Fultz, Phys. Rev. B **84**, 054303 (2011).

[10] H. Bao, B. Qiu, Y. Zhang, and X. Ruan, J. Quant. Spectrosc. Radiat. Transfer **113**, 1683 (2012).

[11] G. Fugallo, B. Rousseau, and M. Lazzeri, Phys. Rev. B **98**, 184307 (2018).

[12] D. A. Broido, M. Malorny, G. Birner, N. Mingo, and D. A. Stewart, Appl. Phys. Lett. **91**, 231922 (2007).

[13] L. Lindsay, D. A. Broido, and N. Mingo, Phys. Rev. B **82**, 115427 (2010).

[14] L. Lindsay, D. A. Broido, and T. L. Reinecke, Phys. Rev. Lett. **109**, 095901 (2012).

[15] T. Feng and X. Ruan, Phys. Rev. B **93**, 045202 (2016).

[16] T. Feng, L. Lindsay, and X. Ruan, Phys. Rev. B **96**, 161201(R) (2017).

[17] T. Feng and X. Ruan, Phys. Rev. B **97**, 045202 (2018).

[18] A. Kundu, N. Mingo, D. A. Broido, and D. A. Stewart, Phys. Rev. B **84**, 125426 (2011).

[19] A. A. Maradudin and A. E. Fein, Phys. Rev. **128**, 2589 (1962).

[20] A. Ward, D. A. Broido, D. A. Stewart, and G. Deinzer, Phys. Rev. B **80**, 125203 (2009).

[21] G. Kresse and J. Furthmüller, Comput. Mater. Sci. **6**, 15 (1996).

[22] See Supplemental Material at http://link.aps.org/supplemental/10.1103/PhysRevB.101.161202 for the computational details, phonon dispersions for all of the materials examined in this work, and Raman spectroscopy characterization.

[23] J. S. Kang, M. Li, H. Wu, H. Nguyen, and Y. Hu, Science **361**, 575 (2018).

[24] S. Li, Q. Zheng, Y. Lv, X. Liu, X. Wang, P. Y. Huang, D. G. Cahill, and B. Lv, Science **361**, 579 (2018).

[25] F. Tian, B. Song, X. Chen, N. K. Ravichandran, Y. Lv, K. Chen, S. Sullivan, J. Kim, Y. Zhou, T.-H. Liu *et al.*, Science **361**, 582 (2018).

[26] Y. Xia, Appl. Phys. Lett. **113**, 073901 (2018).

[27] N. K. Ravichandran and D. Broido, Phys. Rev. B **98**, 085205 (2018).

[28] G. Irmer, M. Wenzel, and J. Monecke, Phys. Status Solidi B **195**, 85 (1996).

[29] T. Luo, J. Garg, J. Shiomi, K. Esfarjani, and G. Chen, Europhys. Lett. **101**, 16001 (2013).

[30] L. Lindsay, D. A. Broido, and T. L. Reinecke, Phys. Rev. B **87**, 165201 (2013).

[31] Y. P. Joshi, M. D. Tiwari, and G. S. Verma, Phys. Rev. B **1**, 642 (1970).

[32] W. Borer, S. Mitra, and K. Namjoshi, Solid State Commun. **9**, 1377 (1971).

[33] H. Herchen and M. A. Cappelli, Phys. Rev. B **43**, 11740 (1991).

[34] M. Balkanski, R. F. Wallis, and E. Haro, Phys. Rev. B **28**, 1928 (1983).

[35] J. Menendez and M. Cardona, Phys. Rev. B **29**, 2051 (1984).

[36] C. Ulrich, A. Debernardi, E. Anastassakis, K. Syassen, and M. Cardona, Phys. Status Solidi B **211**, 293 (1999).

[37] K. J. Dean, W. F. Sherman, and G. R. Wilkinson, Spectrochim. Acta, Part A **38**, 1105 (1982).

[38] F. Gervais and B. Piriou, Phys. Rev. B **11**, 3944 (1975).

[39] V. G. Hadjiev, M. N. Iliev, B. Lv, Z. F. Ren, and C. W. Chu, Phys. Rev. B **89**, 024308 (2014).

[40] O. Hellman, P. Steneteg, I. A. Abrikosov, and S. I. Simak, Phys. Rev. B **87**, 104111 (2013).

[41] Z. Tong, L. Liu, L. Li, and H. Bao, Phys. B (Amsterdam, Neth.) **537**, 194 (2018).

Supplemental Material for "Observation of strong higher-order lattice anharmonicity in Raman and infrared response"

Xiaolong Yang*,[1,2,3] Tianli Feng*,[1] Joon Sang Kang,[4] Yongjie Hu,[4] Ju Li,[5] and Xiulin Ruan†[1]

[1]*School of Mechanical Engineering and the Birck Nanotechnology Center, Purdue University, West Lafayette, Indiana 47907-2088, USA.*

[2]*Institute for Advanced Study, Shenzhen University, Shenzhen 518060, China.*

[3]*Frontier Institute of Science and Technology, and State Key Laboratory for Mechanical Behavior of Materials, Xi'an Jiaotong University, Xi'an 710049, China.*

[4]*School of Engineering and Applied Science, University of California, Los Angeles (UCLA), Los Angeles, CA 90095, USA.*

[5]*Department of Nuclear Science and Engineering and Department of Materials Science and Engineering, Massachusetts Institute of Technology, Cambridge, Massachusetts 02139, USA.*

(Dated: March 6, 2020)

A. Computational details

All the IFCs were calculated via real-space finite displacement difference method, with 0.01Å of the magnitude of displacements. The second-order IFCs and phonon frequencies were calculated using $5 \times 5 \times 5$ supercells within the DFT, as implemented in the open-source software packages Phonopy [1]. To capture LO/TO splitting the non-analytical term was involved. The third-order IFCs were calculated through Thirdorder [2], a package of ShengBTE, considering up to the fifth nearest neighbor. The fourth-order IFCs were calculated by using the in-house code, considering up to the second nearest neighbors. The third- and fourth-order IFCs for all of materials examined in this work except α-quartz were performed using $4 \times 4 \times 4$ primitive cells and $4 \times 4 \times 4$ Monkhorst-Pack grid. For α-quartz, we use a $5 \times 5 \times 2$ supercell to calculate the second-order IFCs with $3 \times 3 \times 5$ **q**-mesh, while both of third- and fourth-order IFCs were computed using $3 \times 3 \times 2$ primitive cells. DFT calculations were performed using the VASP [3, 4] using the LDA for exchange and correlation and the projector-augmented-wave method [5]. The plane-wave energy cutoff of all the materials was determined by adding 30% to the highest energy cutoff for the pseudopotentials. Cell parameters and internal atomic positions were fully relaxed until the total energy and maximum ionic Hellmann-Feynman force converge to 10^{-10} eV and 10^{-6} eV/Å, respectively. The phonon linewidth for all materials studied except Ge were taken with a $16 \times 16 \times 16$ **q**-mesh in the first Brillouin zone, which has been proven to make phonon scattering rates converge [6]. As for Ge, we adopted $32 \times 32 \times 32$ **q**-mesh to obtain converged phonon linewidths.

Considering that the large computational cost and the high memory requirement are needed for third- and fourth-order IFCs calculations, herein we harnessed the space-group symmetries of all crystals by calling the Atsushi Togo's spglib which can greatly reduce the required number of DFT calculations. In addition, it is noteworthy that numerical uncertainties will cause small violations in crystal translational and rotational invariance constraints that has a large influence on phonon scattering calculation. To overcome this issue we employed a Lagrange-multiplier symmetrization technique.

[∗] These authors contributed equally to this work.
[†] Corresponding author: ruan@purdue.edu.

B. Phonon dispersions for all of materials

To perform the phonon linewidth and infrared optical property calculations, the accurate phonon frequencies and the corresponding eigenvectors are required, which can be extracted from diagonalization of the dynamical matrix. Here we present the calculated phonon dispersions in the high-symmetry directions for all of the materials considered in this work, along with available experimental data for comparison(see Figs. S1–S7).

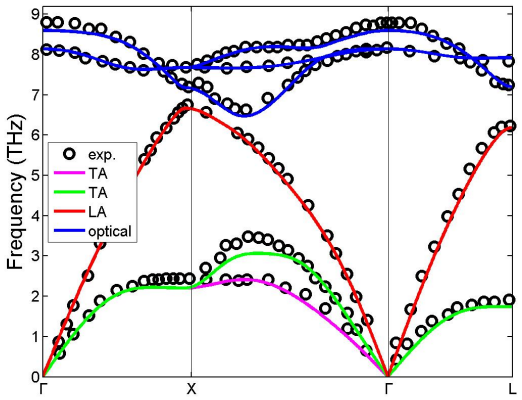

FIG. S1: Calculated phonon dispersion for GaAs in the high symmetry directions (solid curves). Experimental data are given by black circles from Ref. [7].

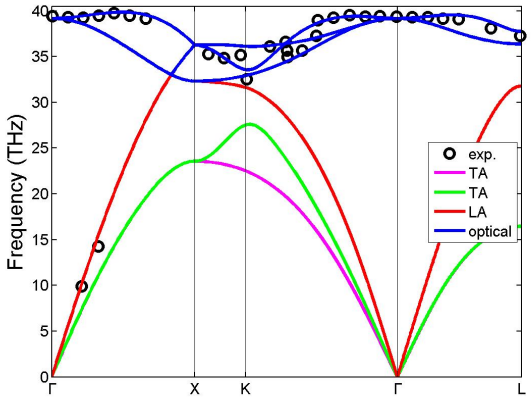

FIG. S2: Calculated phonon dispersion for diamond in the high symmetry directions (solid curves). Experimental data are given by black circles from Ref. [8].

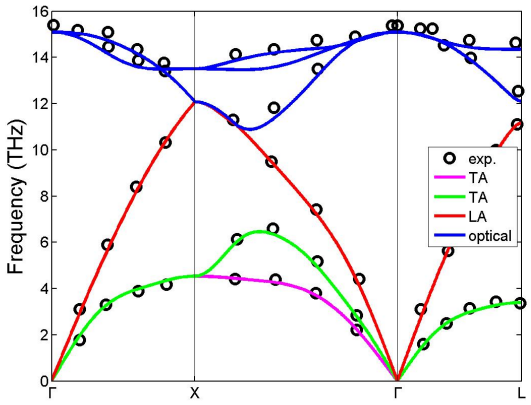

FIG. S3: Calculated phonon dispersion for Si in the high symmetry directions (solid curves). Experimental data are given by black circles from Ref. [9].

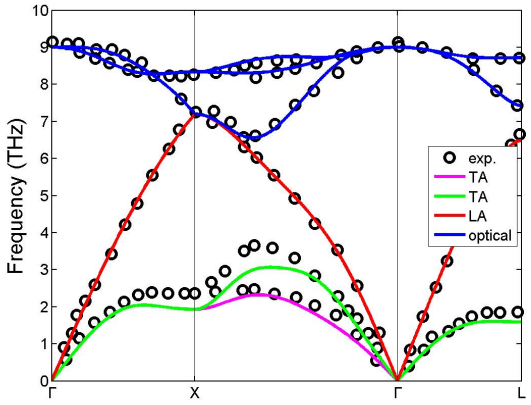

FIG. S4: Calculated phonon dispersion for Ge in the high symmetry directions (solid curves). Experimental data are given by black circles from Ref. [10].

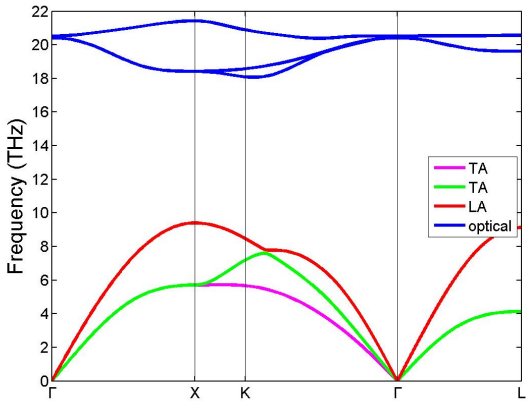

FIG. S5: Calculated phonon dispersion for BAs in the high symmetry directions (solid curves).

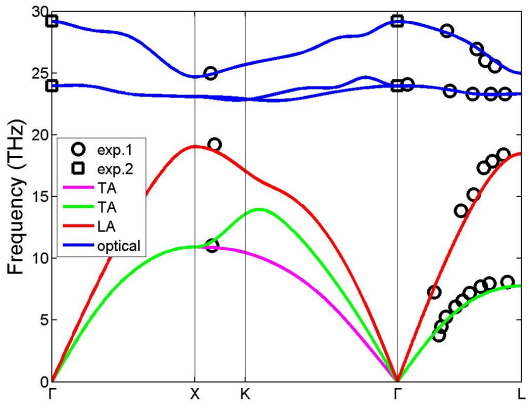

FIG. S6: Calculated phonon dispersion for 3C-SiC in the high symmetry directions (solid curves). Experimental data are given by black circles from Ref. [11] and by black square from Ref. [12].

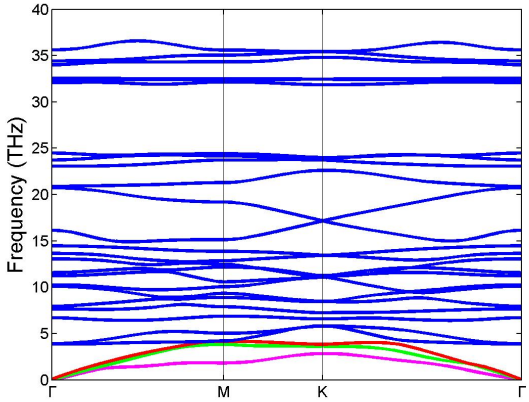

FIG. S7: Calculated phonon dispersion for α-quartz in the high symmetry directions.

Table S1 lists our calculated frequencies at $\mathbf{\Gamma}$ point along with the values of ϵ_∞ for each material considered in this work, comparing with the existing experimental data.

TABLE S1: The optical phonon frequencies (in the unit of cm^{-1}) at the $\mathbf{\Gamma}$ point, along with static dielectric constant ϵ_∞ for all of the materials listed in this work.

Materials	TO mode		LO mode		ϵ_∞	
	Present	Expt.	Present	Expt.	Present	Expt.
GaAs	270.8	267.5 [13]	287.89	285.2 [13]	13.7426	12.85 [14]
BAs	680	-	683.5	-	9.823	-
3C-SiC	799	798 [12]	969	973 [12]	6.924	6.95 [15]
α-quartz	341.7	364 [16]	374.1	387 [16]	2.54	2.383 [16]
α-quartz	482.2	495 [16]	558.4	552 [16]	2.54	2.383 [16]
α-quartz	768.3	777 [16]	790.4	790 [16]	2.54	2.383 [16]
α-quartz	1083.5	1071 [16]	1217.7	1229 [16]	2.54	2.383 [16]

C. Raman spectroscopy characterization

The Raman spectra of both natural abundance and isotope pure BAs were measured using Raman spectroscope (inVia, Renishaw). The laser wavelength is 633nm with 1200/mm grating system. The incident laser was polarized and backscattered. We use $\times$20 objective lens to excite laser and collect signal. Our measured full width at half maximum (FWHM) as a function of temperature for both natural abundance and isotope-pure BAs are shown in Fig.S8. This two data show very similar temperature dependence, and their difference are mainly attributed to the isotope scattering. To highlight only the temperature-dependent anharmonic effects, in Fig.2(a) of the main text we have subtracted the contribution of temperature-independent scattering sources from the original experimental data for comparison.

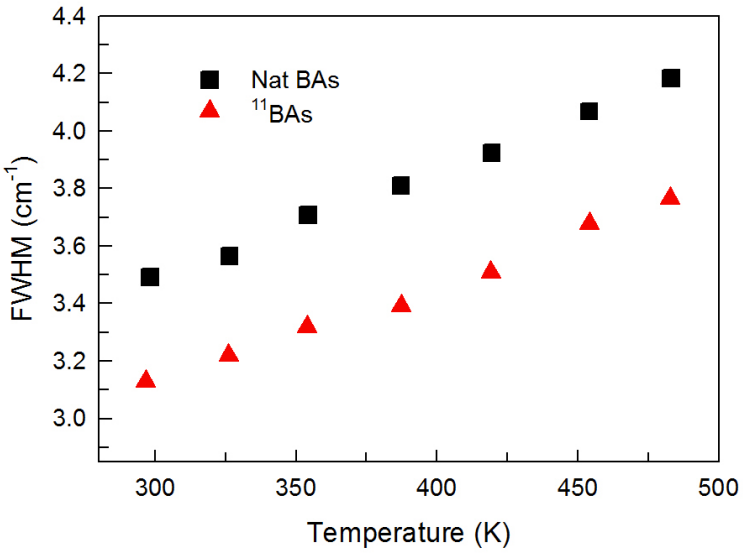

FIG. S8: Temperature dependent full width at half maximum (FWHM) of both natural abundance and isotope pure BAs.

---

[1] A. Togo, F. Oba, and I. Tanaka, Phys. Rev. B **78**, 134106 (2008), URL `https://link.aps.org/doi/10.1103/PhysRevB.78.134106`.

[2] W. Li, J. Carrete, N. A. Katcho, and N. Mingo, Computer Physics Communications **185**, 1747 (2014), ISSN 0010-4655, URL `http://www.sciencedirect.com/science/article/pii/S0010465514000484`.

[3] G. Kresse and J. Hafner, Phys. Rev. B **47**, 558 (1993), URL `https://link.aps.org/doi/10.1103/PhysRevB.47.558`.

[4] G. Kresse and J. Furthmller, Computational Materials Science **6**, 15 (1996), ISSN 0927-0256, URL `http://www.sciencedirect.com/science/article/pii/0927025696000080`.

[5] J. P. Perdew, K. Burke, and M. Ernzerhof, Phys. Rev. Lett. **77**, 3865 (1996), URL `https://link.aps.org/doi/10.1103/PhysRevLett.77.3865`.

[6] T. Feng, L. Lindsay, and X. Ruan, Phys. Rev. B **96**, 161201 (2017), URL `https://link.aps.org/doi/10.1103/PhysRevB.96.161201`.

[7] D. Strauch and B. Dorner, Journal of Physics: Condensed Matter **2**, 1457 (1990), ISSN 0953-8984, URL `http://stacks.iop.org/0953-8984/2/i=6/a=006`.

[8] M. Schwoerer-Bohning, A. T. Macrander, and D. A. Arms, Phys. Rev. Lett. **80**, 5572 (1998), URL https://link.aps.org/doi/10.1103/PhysRevLett.80.5572.

[9] F. H. Stillinger and T. A. Weber, Phys. Rev. B **31**, 5262 (1985), URL https://link.aps.org/doi/10.1103/PhysRevB.31.5262.

[10] K. Ding and H. C. Andersen, Phys. Rev. B **34**, 6987 (1986), URL https://link.aps.org/doi/10.1103/PhysRevB.34.6987.

[11] D. W. Feldman, J. H. Parker, W. J. Choyke, and L. Patrick, Phys. Rev. **173**, 787 (1968), URL https://link.aps.org/doi/10.1103/PhysRev.173.787.

[12] C. Ulrich, A. Debernardi, E. Anastassakis, K. Syassen, and M. Cardona, phys. stat. sol. (b) **211**, 293 (1999), ISSN 0370-1972, URL https://doi.org/10.1002/(SICI)1521-3951(199901)211:1<293::AID-PSSB293>3.0.CO;2-O.

[13] J. S. Blakemore, Journal of Applied Physics **53**, R123 (1982), https://doi.org/10.1063/1.331665, URL https://doi.org/10.1063/1.331665.

[14] H. Bao and X. Ruan, International Journal of Heat and Mass Transfer **53**, 1308 (2010), ISSN 0017-9310, URL http://dx.doi.org/10.1016/j.ijheatmasstransfer.2009.12.033.

[15] Z. Tong, L. Liu, L. Li, and H. Bao, Physica B: Condensed Matter **537**, 194 (2018), ISSN 0921-4526, URL http://www.sciencedirect.com/science/article/pii/S092145261830142X.

[16] F. Gervais and B. Piriou, Phys. Rev. B **11**, 3944 (1975), URL https://link.aps.org/doi/10.1103/PhysRevB.11.3944.